Review

Superlyophilic Interfaces Assisted Thermal Management

LUO Xianfeng[1,2], ZHU Zhongpeng[3]✉, YOU Jun[1]✉, TIAN Ye[2,4] and JIANG Lei[2,4]✉

Received February 26, 2022
Accepted March 22, 2022

Thermal management has become a critical issue owing to the increasing need for various devices including heat dissipation and adsorption. Recently, the rapid growth of scientific reports is seen to improve thermal management efficiency by developing materials with high transfer coefficient and surface improvement to enhance heat transfer rate. Inspired by nature, constructing superlyophilic interfaces has been proved to be an effective way for thermal management and applied in industry and daily life. Herein, state-of-the-art developments of superlyophilic interfaces assisted thermal management are reported mainly from four perspectives around boiling, evaporation, radiation, and condensation. In particular, we discussed the unique role of superlyophilic interfaces during the heat transfer process, such as increasing bubble detachment rate, superspreading assisted efficient evaporation, directional liquid transfer in textiles during radiative cooling, and so forth. Finally, challenges of thermal management assisted by superlyophilic interfaces toward future applications are presented.

Keywords Superhydrophilic; Boiling heat transfer; Evaporation; Radiative cooling; Condensation

1 Introduction

Thermal management of heat dissipation and adsorption is widely needed in various fields including microelectronics, clothes, desalination, etc.[1−4]. To improve the heat transfer efficiency, several key factors need to be considered along the heat transfer process, which are the onset of nucleate boiling(ONB), critical heat flux(CHF), heat transfer coefficient (HTC), and Leidenfrost point(LFP)[5]. Recent studies revealed that constructing superlyophilic surfaces could help to manipulate these factors[6,7]. For the evaporation cooling process, owing to the strong interaction between the cooling liquid and superlyophilic solid substrates, liquids can spread to a large area, which enhances the evaporation heat transfer efficiency[8]. For boiling heat transfer, it is believed that the construction of superlyophilic surfaces can delay the triggering of CHF owing to the rewetting of dry spots and suppress the formation of air film to improve the performance of devices with high power output[9]. The generation of superlyophilic surfaces with strong liquid absorption properties can enhance the heat dissipation efficiency of clothes for passive radiative cooling[10]. Besides, delicate fabrication combining superhydrophilic and superhydrophobic surfaces can improve the condensation heat transfer efficiency[11].

Superlyophilic surfaces denote materials with apparent contact angles being near 0° for various liquids, including superhydrophilic, superoleophilic, and superamphiphilic surfaces[12,13]. It was first systemically studied by Fujishima and his co-workers[14,15] based on UV-induced superamphiphilic titanium dioxide coatings. Since then, superlyophilic surfaces are widely explored and applied in various fields including self-cleaning, anti-fogging, gree-printing, film fabrication, and so forth[16−22]. Generally, the fabrication methods of superlyophilic surfaces can be listed as two categories, physical method and chemical method. In terms of physical method, commonly used methods are physical vapor deposition, electrospinning, and phase separation, etc. In terms of chemical method, commonly used methods are sol-gel, UV illumination, plasma, and chemical vapor deposition, etc.[23−25]. The key mechanism for the construction of superlyophilic surfaces from the perspective of surface chemistry is to generate oxygen vacancy and highly charged ionic elements[26,27]. In addition, developing three-dimensional capillary structures can preserve the superlyophilic property for a relatively long period[8]. Based on these previous studies, we focused on thermal management assisted by superlyophilic interfaces[28−31].

In this study, we summarized the state-of-the-art reports for thermal management assisted by superlyophilic interfaces, interpreting based on five typical heat transfer processes namely boiling, evaporation, radiation, condensation, and integrated properties(Fig.1). First of all,

✉ YOU Jun
youjun@hrbust.edu.cn
✉ ZHU Zhongpeng
zhuzp@buaa.edu.cn
✉ JIANG Lei
jianglei@iccas.ac.cn
1. Key Laboratory of Green Chemical Engineering and Technology of College of Heilongjiang Province, College of Materials Science and Chemical Engineering, Harbin University of Science and Technology, Harbin 150080, P. R. China;
2. Key Laboratory of Bio-inspired Smart Interfacial Science and Technology, Ministry of Education, School of Chemistry, Beihang University, Beijing 100191, P. R. China;
3. Key Laboratory of Bio-inspired Materials and Interfacial Science, Technical Institute of Physics and Chemistry, Chinese Academy of Sciences, Beijing 100190, P. R. China;
4. School of Future Technology, University of Chinese Academy of Sciences, Beijing 101407, P. R. China

https://doi.org/10.1007/s40242-022-2063-4

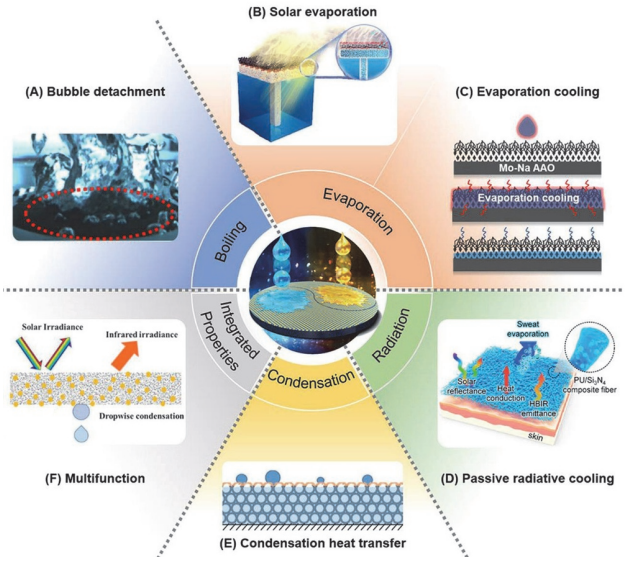

Fig.1 Schematic diagram of the typical superlyophilic interface in thermal management with a wide range of applications

(A) Metal superhydrophilic interface assists the efficient detachment of bubbles; (B) superhydrophilic interface assists endothermic photoevaporation; (C) evaporative heat dissipation due to superspreading properties; (D) superhydrophilic assisted heat dissipation at the interface of fabrics and other solid materials; (E) superhydrophilic liquid interface assisted efficient condensation heat dissipation; (F) multifunctional integrated heat dissipation with superlyophilic properties.

(A) Reprinted with permission from Ref.[32], Copyright 2020, American Chemical Society; (B) reprinted with permission from Ref.[33], Copyright 2021, AIP Publishing; (C) reprinted with permission from Ref.[8], Copyright 2021, Elsevier; (D) reprinted with permission from Ref.[10], Copyright 2022, American Chemical Society; (E) reprinted with permission from Ref.[11], Copyright 2018, Wiley-VCH; (F) reprinted with permission from Ref.[34], Copyright 2022, Elsevier.

superlyophilic interfaces enhanced air bubble detachments are discussed for boiling heat transfer around metal and non-metal substrates. Secondly, solar evaporation of heat adsorption and superspreading enhanced evaporation cooing of heat dissipation are discussed. Thirdly, superlyophilic surface assisted effective liquid adsorption for improved water gas transportation in textiles and other materials of radiative cooling is presented. Meanwhile, the improvement of condensation for water vapor in water collection is briefly summarized. Besides, integrated properties of multifunctional superlyophilic surfaces combining several heat transfer processes are also discussed. Finally, challenges and further outlooks of thermal management assisted by superlyophilic interfaces are presented.

2 Thermal Management of Boiling Process Assisted by Superlyophilic Interfaces

Enhanced boiling is the most efficient form of heat transfer[35−38]. It is implemented in a wide range of power generation and thermal management equipment, such as the cooling of nuclear power plants[37], refrigeration[2], electronics[39], and chemical reactors[40]. Surface wettability has a significant effect on boiling heat transfer. Surfaces with hydrophilic or superhydrophilic properties form a continuous water film, which retards the formation of a vapor film during boiling, thereby increasing CHF. Numerous studies on hydrophilic/superhydrophilic nanorods, nanowires, and carbon nanotubes vertically aligned nanorods have shown significant improvements in boiling heat transfer with both high CHF and high HTC[41]. This improvement is mainly due to the increased density of nucleation sites, as well as the high surface tension of the superhydrophilic nanostructures. Furthermore, studies have shown that surfaces with mixed hydrophilic and hydrophobic micropatterns cause enhanced pools to boil to almost the same extent. The combination of these two wettability prevents the formation of vapor films by attracting liquid to hydrophilic regions, while promoting nucleation in hydrophobic regions. This helps to remove air bubbles efficiently[42].

2.1 Superhydrophilic Metal Interfaces Assisted Efficient Bubble Detachment

In the past decades of research, in order to improve energy utilization and heat dissipation efficiency, the research on super-friendly interface-assisted heat dissipation of metal interfaces has attracted extensive attention. In recent years, due to the excellent electrical and thermal conductivity of metal materials, the desorption of boiling bubbles has become more and more popular[43,44].

The boiling heat transfer field has been studied for a long time. Wu *et al*.[32] reported a copper-based ultrathin and efficient boiling heat transfer(BHT) interface by electroplating copper nanocone cores and low thermal conductivity nickel nanocone coverings(Fig.2). S5 is the sample number of this work, which showed the best performing. The optimized BHT interface can be obtained by adjusting the surface morphology, wettability, boiling point quality, and heat transfer properties of the layered structure. Compared with the flat copper surface, the maximum value of HTC is enhanced by 228%, CHF is enhanced by 71%, and the ONB ultra-high heat is reduced by 68%.

A highly efficient BHT interface based on a superhydrophilic copper microcavity and nanocone(CMN) composite structure was introduced by Ze *et al*.[9]. By exploring the morphology, wettability, boiling quality, and heat transfer performance of the CMN structure as a function of growth time, the best interface was obtained with a maximum enhancement of 142% for HTC, 64% for CHF, and 64% for ONB compared to a flat copper surface. Overheating has been reduced by 33%. This remarkable performance can be attributed to the rational design of the CMN structure, easier bubble nucleation, more nucleation sites, reduced bubble exit

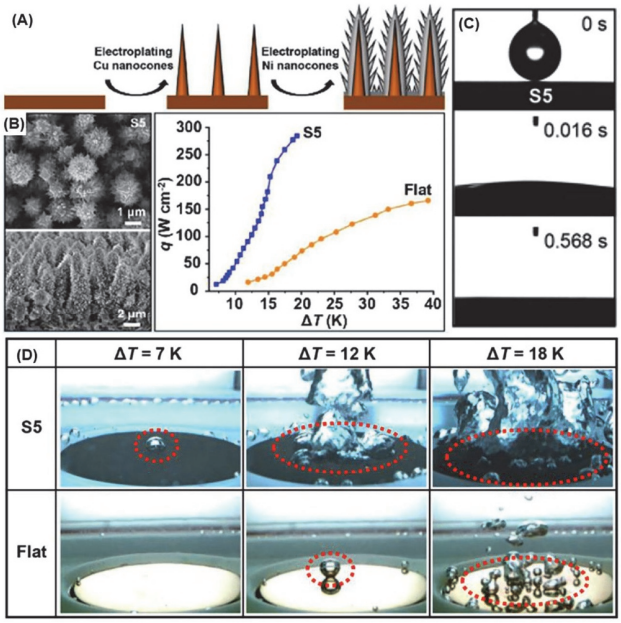

Fig.2 Schematic diagram of the preparation of superlyophilic Cu-Ni nanocones, the heat dissipation effect and the assisted bubble detachment process

(A) Cu-Ni multilayer nanocones were prepared by eletroplaiting; (B) SEM image of the as-prepared nanocones structure and the heat flux(q) *versus* superheat(ΔT) curve of the interface between the prepared sample surface and the flat Cu surface; (C) water droplets can spread completely within 0.568 s; (D) boiling phenomena of the prepared sample interface and the flat Cu interface, which indicates that the interface of the prepared samples is more favorable for bubble departure as ΔT increases.

Reprinted with permission from Ref.[32], Copyright 2020, American Chemical Society.

diameter, increased bubble renewal frequency, enhanced liquid supply, and reduced additional interfacial heat resistance. In contrast to micro-sized and nano-sized structures, micro-nanocomposite structures are more likely to induce interfacial superlyophilicity. Kim *et al*.[45] reported a micro-nanocomposite interface composed of octagonal micropillar arrays and ZnO nanorods, which showed a contact angle of 0°. This micro-nano composite interface shows a significant enhancement in CHF compared to a flat interface, a single micro-scale interface or a nano-scale interface, which is due to the enhanced wettability of the CHF, while the small contact angle is more conducive to the separation of bubbles from the interface. Classical superhydrophilic materials have also been reported by Takata *et al*.[46], which investigated the effect of titanium dioxide(TiO_2) coating as a typical photoresponsive superhydrophilic material on heat transfer properties. Comparing the two surfaces with and without TiO_2 coating, it was found that the CHF was about twice as high as that of the uncoated surface. Also, Kondou *et al*.[47] reported the boiling heat dissipation experiments of several cooling liquids on different hydrophilic interfaces on Cu materials, and the results showed that the difference of cooling liquids on the bare surface and the superhydrophilic surface treated by laser would affect the final heat dissipation effect. Under the defined coolant conditions, the superhydrophilic surface exhibited superiority over other interfaces of HTC and CHF.

2.2 Superhydrophilic Nonmetallic Interfaces Assisted Efficient Bubble Detachment

In terms of non-metallic materials, Si materials are often the main materials. By changing the surface roughness, surface modification, adding micro- and nano-sized structures, etc., CHF and interfacial bubble flow are enhanced[48].

To enhance CHF, Chen *et al*.[49] reported that the high surface tension provided by the liquid in nanowire arrays made of Si and Cu can be used to increase CHF and HTC by more than 100%(Fig.3). It is observed that both the critical heat flux and the thermal conductance on the nanowires are significantly enhanced compared to those of the ordinary surfaces. This enhancement can be attributed to some unique properties of nanowires, such as higher nucleation site density, superhydrophilicity, and enhanced capillary pumping effect. This study demonstrates that CHF and HTC can be further enhanced by rational design and synthesis of nanowire arrays.

Also, in the field of enhancing CHF, Shim *et al*.[50] reported a regularly-arranged silicon nanowire array, which has a higher coolant supply capacity and can further enhance the cooling effect of the cooling liquid, compared with the conventional random-arranged silicon nanowire arrays. This work proposes the concept of volumetric moisture absorption rate, which expresses the supply characteristics of the coolant by considering the liquid supply rate and the addition amount of the coolant and confirms that CHF increases with the increase of the volumetric moisture absorption rate. At the same time, by increasing the length of the silicon nanowires and changing the arrangement spacing, the CHF can be

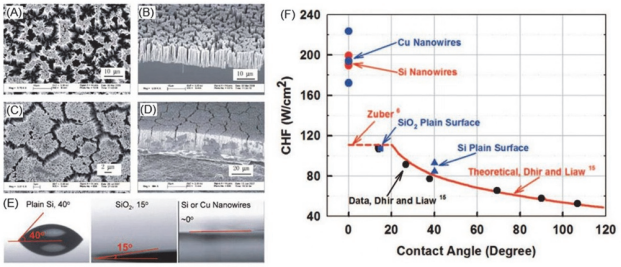

Fig.3 Schematic diagram of successfully prepared Si, Cu nanowires and their CHFs

(A) Top view of Si nanowires; (B) cross section of Si nanowires; (C) top view of Cu nanowires; (D) cross section of Cu nanowires; (E) contact angle images of water droplets on Si, SiO_2, Si or Cu nanowire surfaces(the contact angle of the flat Si interface shows 40°, the SiO_2 surface shows 15°, and the two nanowire arrays show 0°); (F) relationship between CHFs and various interfacial with different contact angles, which indicates that the CHF of surfaces with contact angle near 0° is significantly higher than those of other surfaces.

Reprinted with permission from Ref.[49], Copyright 2009, American Chemical Society.

https://doi.org/10.1007/s40242-022-2063-4

increased to 245.6 W/cm². Kim *et al*.[51] discussed the advantages of Si nanowires(SiNWs) in thermal stability for boiling heat transfer, using a designed temperature array sensor to evaluate the local and temporal heat transfer properties on vertically aligned nanowire arrays. The effect of the rough morphology and high wetting properties of the nanowires enables reliable heat transfer stability/uniformity and efficient heat dissipation in pool-boiling environments. Compared with ordinary surfaces, SiNWs can also guarantee more than 100% increase in heat dissipation capacity and efficiency. Meanwhile, the work points out that the height of the nanowires affects the generation of byproduct nucleation sites in the micrometer scale, which may be a key factor for the improved heat dissipation under superhydrophilic conditions. The effect of surface wettability with silicon nanowires on the boiling flow pattern was reported by Liu *et al*.[52], and experimentally fabricated microchannels of three different sizes, a hydrophilic surface produced by a plasma etching process, a fluorosilane-modified hydrophobic surface, and a grown-obtained ultra-thin microchannel were reported. Nanowire arrays on wafers with hydrophilic surfaces during gas-liquid-solid growth. In addition to nanowires, nanotube arrays are also used for research. Dai *et al*.[53] reported the synthesis of an interface with hydrophobic-hydrophilic composite wettability by partially oxidizing the pristine functionalized multiwall carbon nanotubes(FMWCNTs) surface to form hydrophilic carboxyl and hydroxyl functional groups on defect sites. The FMWCNTs were treated with fluorine gas to obtain hydrophobic fluorinated FMWCNTs and when compared with the original surface, it was found that the enhancement of boiling heat transfer was mainly caused by the introduced hydrophilicity, and the hydrophilicity exhibited by the material interface could improve the CHF.

3 Thermal Management of Evaporation Process Assisted by Superlyophilic Interfaces

Evaporation tends to be the most common form of heat dissipation, as it can occur in the presence of temperature differences. People's research in this area usually focuses on improving the effect of evaporative heat dissipation by increasing the evaporation area and the heat dissipation rate. The superlyophilic interface-assisted evaporative heat dissipation has been widely studied in recent years[54−58].

3.1 Solar Evaporation Assisted by Superlyophilic Interfaces

Due to the large-scale exploitation and use of coal, oil and other energy sources in recent years, people pay more and more attention to clean energy. Among them, solar energy has entered people's field of vision due to its advantages of simple acquisition, non-polluting and renewable.

The phenomenon of solar-promoted evaporation has been studied. Yin *et al*.[33] reported femtosecond laser-textured superhydrophilic copper foam structures, which demonstrated a strategy for efficient steam generation based on the synergistic effect of solar-driven hot air(Fig.4). The superhydrophilic sponge layer of this evaporator can obtain moisture and transport it to the copper foam layer to accelerate evaporation. The experimental results show that its surface evaporation can accelerate heat dissipation, and the design can adjust the steam generation rate by changing the wind speed. These findings provide a strategy for designing solar-powered high-efficiency steam power systems for desalination and wastewater treatment.

As the same sponge material, Li *et al*.[59] reported a microstructure-controllable melamine/silicone(MS) hybrid sponge prepared by further combining with carbon nanotubes(CNTs) for efficient solar-driven interfacial evaporation. The microstructure and wettability of MS sponges were highly controlled by adjusting the silane concentration. The CNTs@MS has very low thermal conductivity, while its superhydrophilic shell is used to absorb

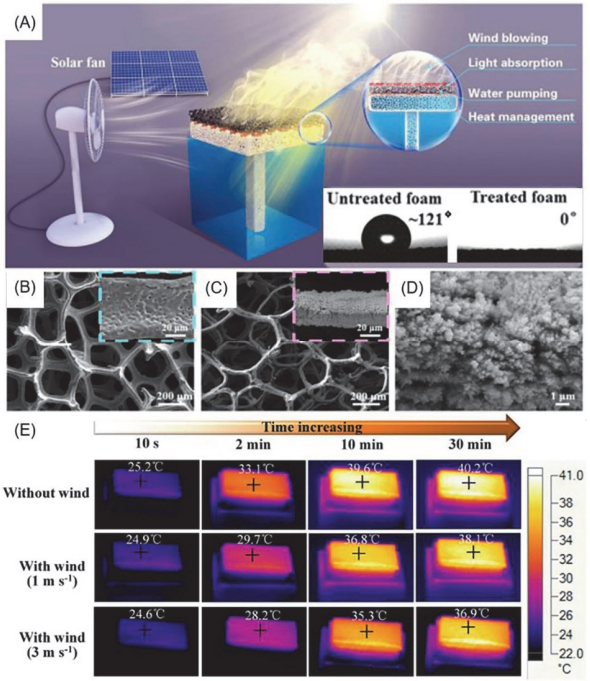

Fig.4 Schematic diagram of the surface of solar-evaporated copper foam structure and the surface heat dissipation that increases with wind speed

(A) Schematic of the operation of the system using solar powered auxiliary evaporation. Water is pumped through the PU sponge into the laser-treated black layer, which can absorb solar energy and be converted into heat. Besides, the evaporation process is further enhanced by wind flow generated over the copper foam surface; (B) SEM image of untreated copper foam; (C) SEM image of the copper foam after laser treatment; (D) high magnification SEM image of the copper foam after laser treatment; (E) evaporative heat dissipation rate of laser-treated copper foam surface at different wind speeds.

Reprinted with permission from Ref.[33], Copyright 2021, AIP Publishing.

https://doi.org/10.1007/s40242-022-2063-4

water, and the superhydrophobic core is used to reduce heat loss and self-floating on the water surface, which can be effectively used in the desalination process for advanced solar evaporators. Zhang *et al.*[60] reported an optimal configuration for enhancing the heat transfer performance of a two-phase closed thermosyphon(TPCT), combining a superhydrophilic (SHi) evaporator and a slip-lubricated porous surface(slip) condenser(TPCT-SHiSL). This study introduced SHi into TPCT to induce superoleophobic behavior of the evaporator, thereby mitigating the boiling/evaporation degradation caused by lubricant pinning. At the same time, the superhydrophilic nature of the evaporator counteracts the contamination and thus degrades the boiling point heat transfer of the residual lubricant due to its superoleophobic nature when immersed in water. An evaporator for efficient and stable seawater desalination named yolk@shell superhydrophobic/superhydrophilic solar evaporator was designed by Hu *et al.*[61]. The vaporizer was fabricated by coating the top surface of a superelastic superhydrophobic silicone sponge with multi-walled carbon nanotubes(MWCNTs) and then changing the outer surface to be superhydrophilic. During the long-term (200 h) continuous Yellow Sea desalination process, the evaporator showed a high and stable evaporation rate of 1.72 $kg·m^{-2}·h^{-1}$ with no salt precipitation on the top surface. Its super salt tolerance comes from the super hydrophilic shell, which can reduce salt in time, reduce salt concentration gradient, and avoid salt precipitation. Bae *et al.*[62] introduced a self-aggregating array of gold-coated alumina nanowires for assisted evaporative heat dissipation under solar radiation. The alumina template prepared by two-step anodization was treated with 5%(mass fraction) phosphoric acid to expand the pore width to obtain self-aggregated alumina nanowire arrays, and the average reflectivity between 2.5 and 17 mm was 7%. Under the illumination of 20 $kW·m^2$, the solar heat conversion efficiency is as high as 57%. On the membrane, the vaporized air bubbles escape directly into the air, while the hydrophilicity of the membrane continuously supplies the surface with underlying water through the micropores. Besides, Wu *et al.*[63] constructed a biomimetic 3D evaporative desalter fabricated by a 3D printing technology for efficient solar-driven water evaporation. Surface-distributed micropores are formed on the prepared surface after being filled with resin, so that the bionic three-dimensional evaporator has ultra-fast water diffusion characteristics. Due to the design morphology of the three-dimensional structure of the asymmetric grooves and the gradient microcavity array, the liquid film diffuses on the surface of the structure, showing a position-dependent liquid film thickness and temperature gradient along the sidewall, which further leads to thermocapillarity within the liquid film, thereby increasing water evaporation and energy efficiency.

3.2 Evaporation Cooling Assisted by Superlyophilic Interfaces

The interface is often chemically modified, the surface structure is changed, and the superlyophilic interface is obtained by its own properties. The superlyophilic interface can provide extremely fast liquid spreading speed, thereby increasing the evaporation area and assisting the liquid to evaporate and dissipate heat.

In terms of alumina materials, Zhu *et al.*[8] reported a superamphiphilic anodic aluminum oxide surface with micro-organized nano-channel(Mo-Na) structures prepared by a single-step anodization method(Fig.5). Taking advantage of the superspreading property of various liquids on the superamphiphilic anodic aluminum oxide surfaces, effective evaporation cooling is demonstrated compared with aluminum plates and traditional hydrophilic anodic aluminum oxide surfaces.

In terms of network structure, Yang *et al.*[44] firstly reported that a micro-nano-sized metal-organic framework film was integrated on a copper mesh to enhance liquid rewetting and capillary-driven heat transfer in evaporation and boiling. This layered multiscale structure utilizes a multiphase transport process to enhance capillary-driven evaporation/boiling of HTCs while increasing CHFs by up to 205%. Since the superhydrophilic HKUST-1 nanopores increase the corresponding interfacial area, the evaporative heat transfer at the liquid-gas interface is significantly improved. Peng *et al.*[64]

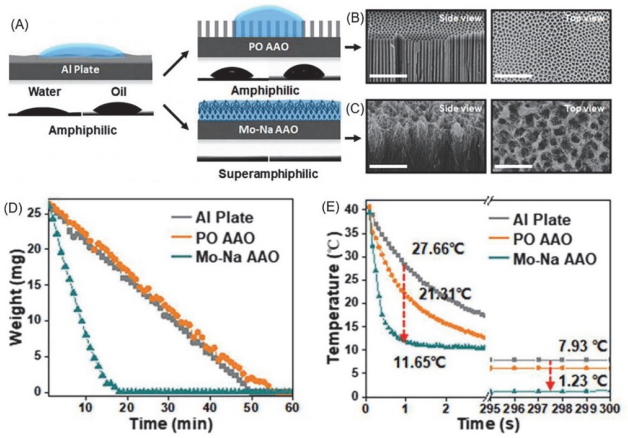

Fig.5 Superhydrophilic spreading on Mo-Na AAO surface and excellent heat dissipation

(A) Amphiphilic porous(PO) anodic aluminum oxide(AAO) surface and superamphiphilic Mo-Na AAO obtained by anodizing method on amphiphilic aluminum(Al) plate surface; (B) SEM image of the tubular structure of the PO AAO surface at 5 μm size; (C) SEM image of three-dimensional interconnected nanochannels on Mo-Na AAO surface at 5 μm size; (D) mass changes of water droplets during evaporation at different surfaces(the evaporation rate of Mo-Na AAO surface is about 3 times higher than that of Al plate and PO AAO surface); (E) temperature changes of water droplets during evaporation at different surfaces.

Reprinted with permission from Ref.[8], Copyright 2021, Elsevier.

https://doi.org/10.1007/s40242-022-2063-4

showed an integrated cooling textile by the combination of Cu foil and Nylon 6 nanofiber films. By rational design, i-Cool exhibits stronger evaporation capacity and higher sweat evaporation cooling efficiency than ordinary textiles. Compared with cotton, the evaporation increase ratio per unit of water is reduced by more than 100%. The integrated cooling textile exhibits fast and steady-state evaporation owing to the effective wicking of perspiration, which provides an effective method for personal perspiration management. Takata *et al*.[65] reported that TiO_2-coated surfaces exposed to UV light exhibited an extremely high affinity for water with a contact angle close to zero. This superhydrophilicity is applied to boiling and evaporative heat transfer, the TiO_2 surface has excellent heat transfer properties in the nucleate boiling region, and its CHF is higher than that of the non-coated surface. The MHF temperature is 100 K higher than that of the uncoated surface. Jiang *et al*.[6] reported the design of structured thermal armour(STA), in which steel columns acted as thermal bridges, embedded with insulating membranes and could pump and diffuse liquid and u-shaped channels for vapour discharge to inhibit the Leidenfrost effect, which can maintain its original heat transfer effect at temperatures up to 1150 °C. The coexistence of materials with different thermal and geometric properties synergistically transforms normally uniform temperatures into non-uniform ones, creating lateral wicks at all temperatures, and enhancing thermal cooling(Fig.6).

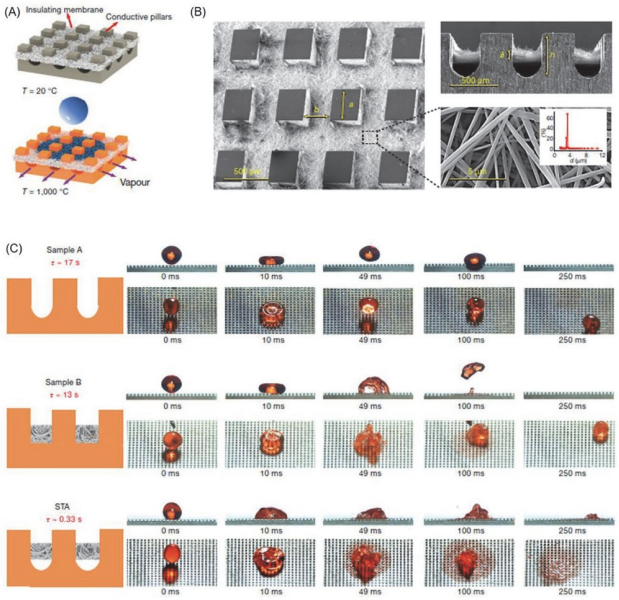

Fig.6 STA design and droplet impact phenomena

(A) STA consists of a series of thick pillars that act as thermal bridges, supporting an insulating superhydrophilic membrane that attracts incoming liquid(this membrane is positioned to create channels, through which vapor can escape); (B) SEM image of the as-prepared STA(the material is made of nano-silicon fibers and is able to resist temperatures around 1200 °C); (C) high-speed camera observation reveals that the Leidenfrost phenomenon of water droplets(stained red, volume 17 μL) occurs on the pillar array(A no membrane), with a little delay on the membrane without channels(B no channel), and in contrast, the water droplets spread continuously on the STA with a temperature of 1000 °C.

Reprinted with permission from Ref.[6], Copyright 2022, Springer Nature.

4 Thermal Management of Radiation Processes Assisted by Superlyophilic Interfaces in Textiles and Other Solid Surfaces

Superlyophilic interfacial treatment also has important applications in radiative cooling[66−70]. For example, after hydrophilic treatment, the inner surface of the fabric can be made hydrophilic so that it can efficiently wick away sweat. In addition, hydrophilic fabrics can also improve the flow of water vapor[71,72].

Recently, relative work has been reported. Miao *et al*.[10] demonstrated a layered polyurethane/Si_3N_4(PU/Si_3N_4) fiber membrane with Janus wettability prepared by a scalable electrospinning method followed by one-sided hydrophilic plasma treatment(Fig.7). Compared with conventional cotton, the high-angle-related solar reflectance(91%) and human infrared emissivity(93%) decreased the temperature by 21.9 °C in direct sunlight and 2.8 °C at night. This extraordinary all-day outdoor cooling performance demonstrates the large temperature cooling effect of PU/Si_3N_4-FM, reducing the risk of human sweat consumption and thermal strain.

Sandwich structures are widely used in fabric design. Song *et al*.[73] prepared a polymer-based nanophotonic textile consisting of a sandwich structure with an inner hydrophilic porous polydopamine modified polyethylene layer, a Si_3N_4@poly(vinylidene fluoride) middle layer, and a hydrophobic polyethylene outer layer. This composite textile shows strong emission of thermal radiation of 8—13 μm and high sunlight reflection of 300—800 nm. Besides, compared

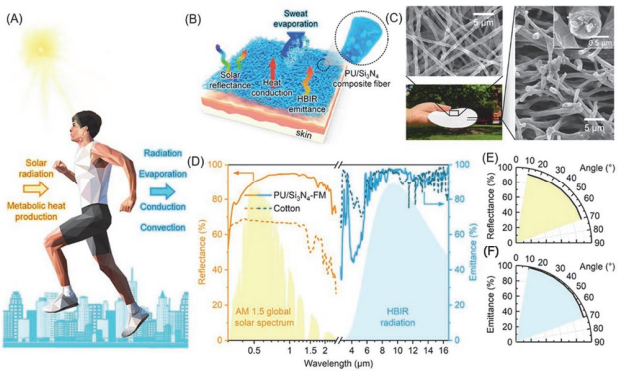

Fig.7 Structure and heat dissipation effect of layered PU/Si_3N_4-FM

(A) Schematic diagram of heat exchange between the human body and the outdoor environment under sunlight; (B) hierarchically designed PU/Si3N4-FM with polymer/inorganic nanoparticle-embedded bonded fiber composition(high solar reflectance, HBIR emissivity, heat transfer, and exceptional moisture management result in efficient personal cooling); (C) top and cross-sectional views of PU/Si_3N_4-FM; (D) spectral UV-Vis-IR reflectance/emissivity of 200 μm thick PU/Si_3N_4-FM(solid line) and 500 μm thick cotton(dashed line) with normalized air mass(AM) 1.5 global solar spectrum(yellow shaded area) and HBIR radiation(blue shaded area) relative; (E) average solar reflectance of layered PU/Si_3N_4-FM at different incidence angles; (F) HBIR emission of layered PU/Si_3N_4-FM at different incidence angles.

Reprinted with permission from Ref.[10], Copyright 2022, American Chemical Society.

https://doi.org/10.1007/s40242-022-2063-4

with cotton and linen, the reported textile cooled human body 3.1—3.5 °C lower indoor and 7.7—10.8 °C lower under direct solar irradiation. A metafabric that combines mechanical strength, water resistance, and breathability was prepared by Zeng *et al*.[74]. Compared with cotton, its temperature has dropped by at least 2 °C, and compared with other common materials, it has excellent cooling performance. Thanks to its layered morphological design, the fabric has a broadband reflectivity of 92.4% in the solar radiation area(0.3—2.5 mm). Hsu *et al*.[75] developed a textile based on NanoPE by coating polydopamine and using spot welding that promotes effective radiative cooling, with enhanced sufficient air permeability, water absorption, liquid absorption, mechanical strength and abrasion resistance at the same time. He *et al*.[76] established a numerical model to predict the temperature of TiO_2 coating surfaces with a water film, integrated a computational algorithm into a simulation tool, and discussed the usability of the model. The simulation results show that the influence of feed water temperature on the vertical distribution of surface temperature can be ignored when the surface is completely covered by a water film. Building walls with a titanium dioxide coating with a water film can be reduced by 20 °C. Compared with the building walls without water, the indoor air temperature dropped by 2—4 °C. Chen *et al*.[77] developed a mechanically robust passive radiation-cooled lignocellulosic body fabricated by a bottom-up assembly layered technique, resulting in a stable cellulose/silica dispersion. Due to the reflected sunlight and emitted heat effects of cellulose fibers and silica, the obtained lignocellulosic bodies exhibited superior cooling effects by reflecting sunlight and radiating heat to atmospheric windows. The mechanical strength of the constructed cooled lignocellulose volume is more than 8 times that of the pure wood fiber volume, and the average dT can reach 6—8 °C within 24 h. Peng *et al*.[7] reported homogeneous large-scale extruded and continuous nanoporous polyethylene microfibers for industrial fabric production(Fig.8). Nanopores embedded in the fibers can efficiently scatter visible light, making it opaque without affecting transparency in the mid-infrared. Compared with commercial cotton fabrics under the same thickness, nano-cotton fabrics have a good cooling capacity, reducing the temperature of human skin by 2.3 °C, which is equivalent to saving more than 20% of indoor cooling energy. In addition to superior cooling, nanopoly fabrics also show impressive abrasion resistance and durability.

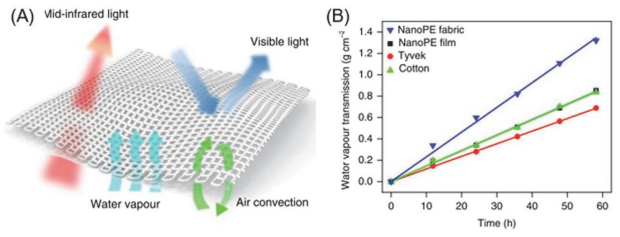

Fig.8 Superhydrophilic nano-vinyl fabric with high water vapour transmission

(A) Schematic diagram of the nano-vinyl fabric, which has high mid-infrared transparency, visible opacity and good abrasion resistance; (B) comparison of water vapour transmission for the four fabrics. NanoPE fabric has the best water vapour transmission significantly higher than other fabrics.

Reprinted with permission from Ref.[7], Copyright 2018, Springer Nature.

5 Thermal Management of Condensation Process Assisted by Superlyophilic Interfaces

In the process of coagulation and heat dissipation, the superlyophilic material interface can easily block efficient heat transfer due to the formation of a water film[78—81]. However, through the design of the hydrophilic and hydrophobic structure, the thickness of the interface liquid film can be controlled, and efficient condensation heat dissipation can also be achieved[5,82—86]. Oh *et al*.[11] reported a hydrophilic-hydrophobic composite film for efficient condensation heat transfer(Fig.9). This film can achieve a heat flux of about 200 $kW \cdot m^{-2} \cdot K^{-1}$ by controlling the coagulation thickness of the film to <10 μm, which improves the durability compared to the classical drop coagulation. A higher solid fraction results in a reduced exposed area for condensation to occur, resulting in a concomitant reduction in heat transfer performance.

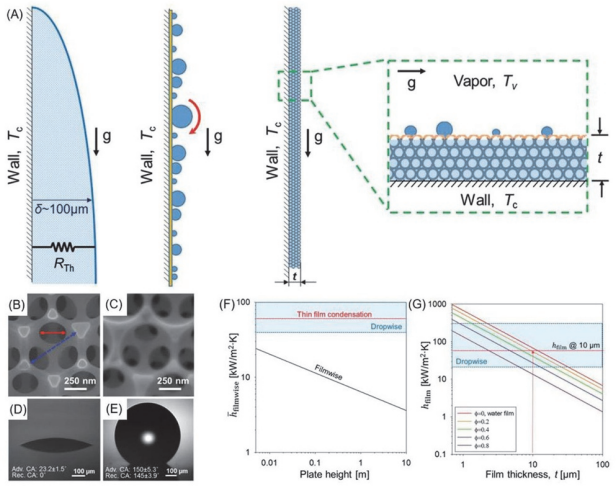

Fig.9 Thin-film condensation heat transfer with a controlled thickness of condensed wafer film

(A) Side-view cross-sectional illustration of film condensation, dropwise condensation(red arrows indicate roll-off and shedding), and a detailed view of a pressurized water film within a superhydrophilic porous structure with a hydrophobic "promoter" coating(orange line); (B) top-view SEM image of the pristine superhydrophilic nickel inverse opals(NIO) surface; (C) top SEM image of the decomposed polyimide after deposition of the hydrophobic surface; (D) the pristine NIO surface shows superhydrophilicity; (E) the hydrophobized surface contact angle can reach *ca*. 150°; (F) average condensation heat transfer coefficient for water vapor as a function of condensation surface height for film, drop and thin film condensation(the thin film condensed structure has a thickness of 10 μm); (G) condensation heat transfer coefficient of thin films as a function of film thickness for different structural solid fractions(as the film thickness increases, the thermal resistance also increases, thereby reducing the heat transfer performance).

Reprinted with permission from Ref.[11], Copyright 2018, Wiley-VCH.

https://doi.org/10.1007/s40242-022-2063-4

In addition to the above-mentioned way of constructing the interface hydrophobic structure to control the liquid film to improve the cohesion and heat dissipation efficiency, there is also a hydrophilic and hydrophobic patterning of the interface to achieve efficient water collection and heat transfer at the same time. Wang *et al*.[86] fabricated hybrid surfaces with superhydrophilic patterns on a superhydrophobic background using photolithography. The droplet kinetics and condensation heat transfer properties of the hybrid surfaces are experimentally investigated and compared with those of fully superhydrophobic, superhydrophobic, and conventional hydrophobic surfaces. By controlling the superhydrophilic pattern length and spacing of the hybrid surface, the droplet diameter, coalescence, and departure frequency can be tuned, resulting in high droplet removal efficiency. Ludwicki *et al*.[87] developed a nanostructured copper oxide surface grafted with poly(*N*-isopropylacrylamide) with switchable superhydrophilic to hydrophobic behavior depending on surface temperature. Two condensation modes can be exhibited. The non-wetting state exhibits dropwise condensation and twice heat transfer coefficient relative to the high-wetting state that produces thin-film condensation. Ji *et al*.[88] prepared a hydrophobic(HPo) surface with a fluorocarbon coating using polytetrafluoroethylene as the matrix resin and micro-nano silica as the additive. A superhydrophilic-hydrophobic(SHPi-HPo) network hybrid surface composed of superhydrophilic network grooves and hydrophobic regions was designed. The results show that the SHPi-HPo surface can effectively control the droplet diameter with an optimal grid spacing of 2.5 mm, and its heat transfer coefficients are 2.7 and 3.4 times higher than those of the HPi and HPo surfaces alone, respectively.

6 Integrated Thermal Management Capabilities Assisted by Superlyophilic Interfaces

In addition, we also found some reports of multi-functional integrated thermal management through research. Integrated thermal management is achieved by combing self-cleaning properties, radiative cooling, condensation or other processes[89−98]. Benlattar *et al*.[99] proposed a new design method for bilayer nanoparticle coatings. The bottom layer is alumina embedded with Ni nanoparticles and the top layer is a superhydrophilic titania-silica layer. The bottom layer is designed to achieve high emissivity. The top layer is designed to block solar lighting and facilitates the cleanliness of the coating design. Liu *et al*.[100] proposed a hydrophilicly durable enhanced specular reflector-metal for effective sub-ambient radiative cooling and dew condensation. The water contact angle of this surface is 22.62°±3.91°, which exhibits a competitive radiative cooling ability compared with durable enhanced specular reflector-metal and polytetra-fluororoethylene and a slightly improved dew condensation efficiency.

Inspired by nature, Chen *et al*.[34] demonstrated a versatile and efficient water collection coating combining daytime radiative cooling and droplet collection techniques, and efficient water collection was achieved by using hydrophobic silica and hydrophilic titania nanospheres at an optimized mass ratio. The coating can simultaneously emit ＞95% thermal IR by reflecting 90% of the incident sunlight, and this high-performance collector coating realized by spectral selectivity and wettability engineering opens a new avenue for the design of high-efficiency water/liquid collecting surfaces(Fig.10).

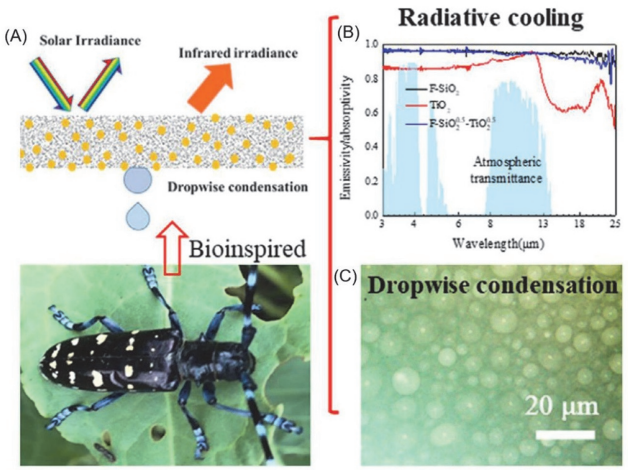

Fig.10 Biomimetic integrated heat management combining irradiative cooling with condensation

(A) A biomimetic composite film inspired by insect elytra with good solar reflectance and infrared emissivity while showing extremely high water production; (B) thermal infrared emissivity on different samples; (C) droplet collection on hydrophilic and superhydrophobic patterned surfaces.

Reprinted with permission from Ref.[34], Copyright 2021, Elsevier.

7 Summary and Outlook

In this review, we have summarized thermal management assisted by superlyophilic interfaces based on boiling, evaporation, radiation, condensation, and other integrated heat transfer processes for various applications. Especially, we focused on several typical thermal management scenarios and discussed the unique role of superlyophilic surfaces during the heat transfer processes, such as enhanced boiling heat transfer owing to the low adhesion of air bubble for superhydrophilic interfaces, effective evaporation cooling resulted from large-area superspreading of liquid droplets on superlyophilic surfaces, directional liquid adsorption for passive radiative cooling in superlyophilic textiles, patterned superhydrophilic/hydrophobic surfaces for enhanced condensation, and integrated heat transfer processes with

https://doi.org/10.1007/s40242-022-2063-4

multifunctions. With these intriguing characteristics, there are certainly tremendous opportunities in future works based on superlyophilic interfaces assisted heat management.

Besides, there are still some remaining challenges for superlyophilic interface assisted thermal management. Owing to the high surface energy, superlyophilic materials are easy to be contaminated, which impeds their practical applications. Besides, some superlyophilic materials are intolerant for extreme conditions, such as high temperature and wear. Hence, developing durable long-term superlyophilic materials is still a challenge. However, with the development of more advanced thermal materials, superlyophilic interfaces assisted thermal management may be further extended to thermal-energy generation and storage, thermal actuation, etc.

Acknowledgements

This work was supported by the National Natural Science Foundation of China (Nos.21988102, 22002005) and the China Postdoctoral Science Foundation (Nos.2019M660397, 2019TQ0014).

Conflicts of Interest

The authors declare no conflicts of interest.

References

[1] Balandin A. A., *Nat. Mater.*, **2011**, *10*(8), 569
[2] Tao P., Shang W., Song C., Shen Q., Zhang F., Luo Z., Yi N., Zhang D., Deng T., *Adv. Mater.*, **2015**, *27*(3), 428
[3] Kwon Y. J., Park J. B., Jeon Y. P., Hong J. Y., Park H. S., Lee J. U., *Polymers(Basel)*, **2021**, *13*(8), 1312
[4] Peng L., Su B., Yu A., Jiang X., *Cellulose*, **2019**, *26*(11), 6415
[5] Patankar N. A., *Soft Matter*, **2010**, *6*(8), 1613
[6] Jiang M. N., Wang Y., Liu F. Y., Du H. H., Li Y. C., Zhang H. H., To S. E., Wang S., Pan C., Yu J. H., Quere D., Wang Z. K., *Nature*, **2022**, *601*(7894), 17
[7] Peng Y. C., Chen J., Song A. Y., Catrysse P. B., Hsu P. C., Cai L. L., Liu B. F., Zhu Y. Y., Zhou G. M., Wu D. S., Lee H. R., Fan S. H., Cui Y., *Nat. Sustain.*, **2018**, *1*(2), 105
[8] Zhu Z., Chen Y., Xu Z., Yu Z., Luo X., Zhou J., Tian Y., Jiang L., *iScience*, **2021**, *24*(4), 102334
[9] Ze H. J., Wu F. F., Chen S. H., Gao X. F., *Adv. Mater. Interfaces*, **2020**, *7*(14), 6
[10] Miao D., Cheng N., Wang X., Yu J., Ding B., *Nano Lett.*, **2022**, *22*(2), 680
[11] Oh J., Zhang R., Shetty P. P., Krogstad J. A., Braun P. V., Miljkovic N., *Adv. Funct. Mater.*, **2018**, *28*(16), 1707000
[12] Zhu Z. P., Zheng S., Peng S., Zhao Y., Tian Y., *Adv. Mater.*, **2017**, *29*(45), 1703120
[13] Wang S., Liu K., Yao X., Jiang L., *Chem. Rev.*, **2015**, *115*(16), 8230
[14] Wang R., Hashimoto K., Fujishima A., Chikuni M., Kojima E., Kitamura A., Shimohigoshi M., Watanabe T., *Nature*, **1997**, *388*, 431
[15] Fujishima A., Zhang X. T., Tryk D. A., *Surf. Sci. Rep.*, **2008**, *63*(12), 515
[16] Zhu Z., Tian Y., Chen Y. P., Gu Z., Wang S. T., Jiang L., *Angew. Chem. Int. Ed.*, **2017**, *56*(21), 5720
[17] Wu L., Dong Z., Kuang M., Li Y., Li F., Jiang L., Song Y., *Adv. Funct. Mater.*, **2015**, *25*(15), 2237
[18] Son J., Kundu S., Verma L. K., Sakhuja M., Danner A. J., Bhatia C. S., Yang H., *Sol. Energy Mater. Sol. Cells*, **2012**, *98*, 46
[19] England M. W., Urata C., Dunderdale G. J., Hozumi A., *ACS Appl. Mater. Interfaces*, **2016**, *8*(7), 4318
[20] Zhang W. B., Zhang F., Gao S. J., Zhu Y. Z., Li J. Y., Jin J., *Sep. Purif. Technol.*, **2015**, *156*, 207
[21] Zhang P. C., Shao N., Qin L. D., *Adv. Mater.*, **2021**, *33*(46), 29
[22] Zhu H., Duan R. L., Wang X. D., Yang J. L., Wang J. H., Huang Y., Xia F., *Nanoscale*, **2018**, *10*(27), 13045
[23] Ye J. M., Yin Q. M., Zhou Y. L., *Thin Solid Films*, **2009**, *517*(21), 6012
[24] Wang R., Sakai N., Fujishima A., Watanabe T., Hashimoto K., *J. Phys. Chem. B*, **1999**, *103*(12), 2188
[25] Vorobyev A. Y., Guo C., *Opt. Express*, **2010**, *18*(7), 6455
[26] Sakai N., Fujishima A., Watanabe T., Hashimoto K., *J. Phys. Chem. B*, **2003**, *107*(4), 1028
[27] Liu M. J., Wang S. T., Jiang L., *Nat. Rev. Mater.*, **2017**, *2*(7), 17036
[28] Schutzius T. M., Bayer I. S., Jursich G. M., Das A., Megaridis C. M., *Nanoscale*, **2012**, *4*(17), 5378
[29] Adera S., Raj R., Enright R., Wang E. N., *Nature Communications*, **2013**, *4*, 1
[30] Wiedenheft K. F., Guo H. A., Qu X., Boreyko J. B., Liu F., Zhang K., Eid F., Choudhury A., Li Z., Chen C.-H., *Applied Physics Letters*, **2017**, *110*(14), 141601
[31] Dai B., Li K., Shi L., Wan X., Liu X., Zhang F., Jiang L., Wang S., *Advanced Materials*, **2019**, *31*(41), 1904113
[32] Wu F. F., Ze H. J., Chen S. H., Gao X. F., *ACS Appl. Mater. Interfaces*, **2020**, *12*(35), 39902
[33] Yin K., Wu Z., Wu J., Zhu Z., Zhang F., Duan J.-A., *Appl. Phys. Lett.*, **2021**, *118*(21), 211905
[34] Chen G., Wang Y., Qiu J., Cao J., Zou Y., Wang S., Jia D., Zhou Y., *Mater. Des.*, **2021**, *206*, 109829
[35] Suroto B. J., Kohno M., Takata Y., *AIP Publishing LLC*, **2018**, *1927*(1), 030047
[36] McClure E. R., Carey V. P., *ACS Appl. Mater. Interfaces*, **2020**, *12*(23), 26350
[37] Moze M., Senegacnik M., Gregorcic P., Hocevar M., Zupancic M., Golobic I., *ACS Appl. Mater. Interfaces*, **2020**, *12*(21), 24419
[38] Lim Y. S., Hung Y. M., *Energy Convers. Manage.*, **2021**, *244*, 114522
[39] Lv L. C., Li J., *Appl. Therm. Eng.*, **2017**, *122*, 593
[40] Li S., Luo X., Li C., *Surf. Coat. Technol.*, **2021**, *422*, 127519
[41] Tang Y., Yang X. L., Li Y. M., Zhu D., *Adv. Mater. Interfaces*, **2021**, *8*(13), 10
[42] Drelich J., Marmur A., *Surf. Innov.*, **2014**, *2*(4), 211
[43] Saneie N., Kulkarni V., Treska B., Fezzaa K., Patankar N., Anand S., *Int. J. Heat Mass Transfer*, **2021**, *176*, 121413
[44] Yang G., Liu J., Cheng X., Wang Y., Chu X., Mukherjee S., Terzis A., Schneemann A., Li W., Wu J., Fischer R. A., *J. Mater. Chem. A*, **2021**, *9*(45), 25480
[45] Kim S., Kim H. D., Kim H., Ahn H. S., Jo H., Kim J., Kim M. H., *Exp. Therm. Fluid Sci.*, **2010**, *34*(4), 487
[46] Takata Y., Hidaka S., Masuda M., Ito T., *Int. J. Energy Res.*, **2003**, *27*(2), 111
[47] Kondou C., Umemoto S., Koyama S., Mitooka Y., *Appl. Therm. Eng.*, **2017**, *118*, 147
[48] Yang F. H., Dai X. M., Peles Y., Cheng P., Khan J., Li C., *Int. J. Heat Mass Transfer*, **2014**, *68*, 703
[49] Chen R., Lu M.-C., Srinivasan V., Wang Z., Cho H. H., Majumdar A., *Nano Lett.*, **2009**, *9*(2), 548
[50] Shim D. II, Choi G., Lee N., Kim T., Kim B. S., Cho H. H., *ACS Appl. Mater. Interfaces*, **2017**, *9*(20), 17595
[51] Kim B. S., Shin S., Lee D., Choi G., Lee H., Kim K. M., Cho H. H., *Int. J. Heat Mass Transfer*, **2014**, *70*, 23
[52] Liu T. Y., Li P. L., Liu C. W., Gau C., *Int. J. Heat Mass Transfer*, **2011**, *54*(1/3), 126
[53] Dai X., Huang X., Yang F., Li X., Sightler J., Yang Y., Li C., *Appl. Phys. Lett.*, **2013**, *102*(16), 161605
[54] Wu S. L., Quan L. N., Huang Y. T., Li Y. T., Yang H. C., Darling S. B., *ACS Appl Mater Interfaces*, **2021**, *13*(33), 39513
[55] Xiao R., Maroo S. C., Wang E. N., *Appl. Phys. Lett.*, **2013**, *102*(12), 123103
[56] Panda A., Pati A. R., Kumar A., Mohapatra S. S., *Int. Commun. Heat Mass Transfer*, **2019**, *105*, 19
[57] Hong S. J., Pialago E. J. T., Ha H. H., Kwon O. K., Park C. W., *Int. J. Heat Mass Transfer*, **2020**, *157*, 119935
[58] Ranjan R., Murthy J. Y., Garimella S. V., *Int. J. Heat Mass Transfer*, **2011**, *54*(1/3), 169
[59] Li L., Li Q., Feng Y., Chen K., Zhang J., *ACS Appl. Mater. Interfaces*, **2021**, *14*(1), 2360
[60] Zhang P., Lv F. Y., Askounis A., Orejon D., Shen B., *Int. J. Heat Mass Transfer*, **2017**, *109*, 1229
[61] Hu T., Li L. X., Yang Y. F., Zhang J. P., *J. Mater. Chem. A*, **2020**, *8*(29), 14736
[62] Bae K., Kang G., Cho S. K., Park W., Kim K., Padilla W. J., *Nat. Commun.*, **2015**, *6*, 10103
[63] Wu L., Dong Z., Cai Z., Ganapathy T., Fang N. X., Li C., Yu C., Zhang Y., Song Y., *Nat. Commun.*, **2020**, *11*(1), 521
[64] Peng Y., Li W., Liu B., Jin W., Schaadt J., Tang J., Zhou G., Wang G., Zhou J., Zhang C., Zhu Y., Huang W., Wu T., Goodson K. E., Dames C., Prasher R., Fan S., Cui Y., *Nat. Commun.*, **2021**, *12*(1), 6122
[65] Takata Y., Hidaka S., Cao J. M., Nakamura T., Yamamoto H., Masuda M., Ito T., *Energy*, **2005**, *30*(2/4), 209

[66] Bai X. H., Li Y. G., Zhang F. Y., Xu Y. Q., Wang S. F., Fu G. S., *Environ. Sci. Water Res. Technol.*, **2019**, *5*(11), 2041
[67] Guo L. P., Gong J., Song C. Y., Zhao Y. L., Tan B. E., Zhao Q., Jin S. B., *ACS Energy Lett.*, **2020**, *5*(4), 1300
[68] He J. X., Zhang Z., Xiao C. H., Liu F., Sun H. X., Zhu Z. Q., Liang W. D., Li A., *ACS Appl. Mater. Interfaces*, **2020**, *12*(14), 16308
[69] Jaleh B., Shariati K., Khosravi M., Moradi A., Ghasemi S., Azizian S., *Colloids Surf. A*, **2019**, *577*, 323
[70] Liu Y. Y., Qian L. Q., Guo C., Jia X., Wang J. W., Tang W. H., *J. Alloys Compd.*, **2009**, *479*(1/2), 532
[71] Aytug T., Simpson J. T., Lupini A. R., Trejo R. M., Jellison G. E., Ivanov I. N., Pennycook S. J., Hillesheim D. A., Winter K. O., Christen D. K., Hunter S. R., Haynes J. A., *Nanotechnology*, **2013**, *24*(31), 315602
[72] Rathousky J., Rohlfing D. F., Wark M., Brezesinski T., Smarsly B., *Thin Solid Films*, **2007**, *515*(16), 6541
[73] Song Y.-N., Lei M.-Q., Deng L.-F., Lei J., Li Z.-M., *ACS Appl. Polym. Mater.*, **2020**, *2*(11), 4379
[74] Zeng S. N., Pian S. J., Su M. Y., Wang Z. N., Wu M. Q., Liu X. H., Chen M. Y., Xiang Y. Z., Wu J. W., Zhang M. N., Cen Q. Q., Tang Y. W., Zhou X. H., Huang Z. H., Wang R., Tunuhe A., Sun X. Y., Xia Z. G., Tian M. W., Chen M., Ma X., Yang L., Zhou J., Zhou H. M., Yang Q., Li X., Ma Y. G., Tao G. M., *Science*, **2021**, *373*(6555), 692
[75] Hsu P. C., Song A. Y., Catrysse P. B., Liu C., Peng Y. C., Xie J., Fan S. H., Cui Y., *Science*, **2016**, *353*(6303), 1019
[76] He J., Hoyano A., *Energy Build.*, **2008**, *40*(6), 968
[77] Chen Y. P., Dang B. K., Fu J. Z., Wang C., Li C. C., Sun Q. F., Li H. Q., *Nano Lett.*, **2021**, *21*(1), 397
[78] Bisetto A., Bortolin S., Del Col D., *Exp. Therm. Fluid Sci.*, **2015**, *68*, 216
[79] Boyina K. S., Mahvi A. J., Chavan S., Park D., Kumar K., Lira M., Yu Y. X., Gunay A. A., Wang X. F., Miljkovic N., *Int. J. Heat Mass Transfer*, **2019**, *145*, 13
[80] Ghosh A., Beaini S., Zhang B. J., Ganguly R., Megaridis C. M., *Langmuir*, **2014**, *30*(43), 13103
[81] Lou D., Liu Q., Mei S., Yang S., Zhai Z., Zheng Z., Cheng J., Liu D., *Surface Technology*, **2019**, *48*(11), 202
[82] Mahapatra P. S., Ghosh A., Ganguly R., Megaridis C. M., *Int. J. Heat Mass Transfer*, **2016**, *92*, 877
[83] Moradi M., Chini S. F., Rahimian M. H., *Aip Advances*, **2020**, *10*(9), 6
[84] Yang K. S., Lin K. H., Tu C. W., He Y. Z., Wang C. C., *Int. J. Heat Mass Transfer*, **2017**, *115*, 1032
[85] Zhou D., Ji X., Dai C., Xu J., *J. Mech. Eng.*, **2018**, *54*(10), 182
[86] Wang H., Zhao X., Wang J., Wang Z., Wang D., Tian J., *Case Stud. Therm. Eng.*, **2021**, *27*, 101319
[87] Ludwicki J. M., Robinson F. L., Steen P. H., *ACS Appl. Mater. Interfaces*, **2020**, *12*(19), 22115
[88] Ji X. B., Zhou D. D., Dai C., Xu J. L., *Int. J. Heat Mass Transfer*, **2019**, *132*, 52
[89] Kang J.-Y., Kim T. K., Lee G. C., Jo H., Kim M. H., Park H. S., *Ann. Nucl. Energy.*, **2019**, *129*, 375
[90] Kang J.-Y., Lee G. C., Kim M. H., Moriyama K., Park H. S., *Int. J. Heat Mass Transfer*, **2018**, *117*, 538
[91] Misyura S. Y., *Int. Commun. Heat Mass Transfer*, **2020**, *112*, 104474
[92] Shen C., Zhang C., Gao M., Li X., Liu Y., Ren L., Moita A. S., *Int. J. Heat Fluid Flow*, **2018**, *74*, 89
[93] Venkitesh V., Dash S., *Int. J. Therm. Sci.*, **2022**, *171*, 107235
[94] Wang J. X., Birbarah P., Docimo D., Yang T. Y., Alleyne A. G., Miljkovic N., *Phys. Rev. E*, **2021**, *103*(2), 14
[95] Xie S., Ma X., Kong H., Bai S., Jiang M., Zhao J., *Int. J. Heat Mass Transfer*, **2021**, *176*, 121475
[96] Xu W., Zhang P., *Int. J. Heat Mass Transfer*, **2020**, *154*, 119642
[97] Zhang J.-Y., Fan L.-W., Li J.-Q., Yu Z.-T., *Int. J. Heat Mass Transfer*, **2020**, *162*, 120364
[98] Zhang J.-Y., Li J.-Q., Jiang L.-Y., Fan L.-W., Yu Z.-T., *Int. J. Heat Mass Transfer*, **2019**, *138*, 1117
[99] Benlattar M., Ibourk I., Adhiri R., *Atmosphere*, **2021**, *12*(9), 1198
[100] Liu C., Fan J., Bao H., *Sol. Energy Mater. Sol. Cells*, **2020**, *216*, 110700